

# Numerical simulation of metal transfer in pulsed-MIG welding

Y. Ogino<sup>1</sup> · Y. Hirata<sup>1</sup> · S. Asai<sup>1</sup>

Received: 30 January 2017 / Accepted: 6 June 2017 / Published online: 20 June 2017  
© International Institute of Welding 2017

**Abstract** Pulsed currents of various shapes have been employed to control the metal transfer phenomena. In the present study, a simulation model including both the arc plasma and the metal transfer is constructed, and their behaviors in pulsed-MIG arc welding are numerically investigated. When the peak current is set to 450 A and the peak time is set to 1.5 ms, only a single droplet is transferred per pulse. The numerical model can indicate the metal transfer and arc plasma behavior depending on the pulse shape. The temperature of the arc plasma increases rapidly at the early phase of the peak time, and consequently, the temperature of the wire electrode increases. After that, a large amount of the metal vapor generates from the wire tip, and the arc temperature decreases. These behaviors are periodic and can be controlled through the pulse shape. In addition, the appropriate pulse frequency depends on the surface tension of the wire electrode. This result shows that balance of the surface tension and the electromagnetic force is important to determine the droplet behavior. Therefore, in controlling the welding process, it is important to consider the properties of both the welding power source and the welding material.

**Keywords (IIW Thesaurus)** Pulsed-MIG arc welding · Numerical simulation · Unified model · Arc plasma · Metal transfer · Metal vapor

Recommended for publication by Study Group 212 - The Physics of Welding

✉ Y. Ogino  
ogino@mapse.eng.osaka-u.ac.jp

<sup>1</sup> Graduate School of Engineering, Osaka University, 2-1 Yamada-oka, Suita, Osaka, Japan

## 1 Introduction

Gas metal arc welding (GMAW) is an indispensable technology used in various areas of industry. GMAW involves metal transfer phenomena because a consumable wire electrode is used. In order to control the quality of the weld, e.g., the shape of weld bead and the strength of the weld, it is very important to control individual welding phenomena. In particular, the properties of the metal transfer, such as the droplet size and the frequency of droplet transfer, strongly affect the stability and quality of the overall process and must be controlled appropriately.

Pulsed current is often used to control the metal transfer phenomena [1–3]. When an appropriate pulse current is set, “one-pulse, one-droplet” transfer is achieved, which provides very stable welding and low spatter. The appropriate pulsed current is typically determined by trial and error. Whereas, the behavior of the droplet during the welding process has been visualized using numerical simulations in order to make clear the phenomena. The early-phase numerical models of the droplet transfer phenomena can be divided into two types. The first type is based on the static force balance theory [4–6], and the second is based on the pinch instability theory [7, 8]. The models based on static force balance theory focus on axial forces acting on the droplet, and the models based on pinch instability theory focus on radial forces. Recently, many dynamic models using CFD have been reported [9–13]. Especially, some numerical model including influence of the arc plasma is constructed and reported [14–16]. For example, Hertel et al. reported numerical results about pulsed-MIG welding. In the paper, detail of the droplet and the arc plasma behavior is calculated, but influence of the current profile is not discussed [17]. Ogino et al. reported numerical results about influence of the shielding gas using continuous current [18].

The objective of the present study is to visualize the phenomena, especially the droplet behavior, in pulsed-MIG welding through numerical simulation. A unified numerical model including both the arc plasma and the droplet is constructed. Using the numerical model, the appropriate peak time (duration for which the pulse is at its peak amplitude) that leads to a one-pulse, one-droplet transfer is selected, and detailed behavior of the arc plasma and the droplet depending on the current profile is numerically visualized. In addition, it is reported that the balance between the electromagnetic force and the surface tension is important to determine the droplet behavior [19]. The surface tension of the wire electrode strongly depends on the chemical components of the wire electrode. The component is designed to obtain appropriate welding results, and so many kinds of the wire material are developed. In this study, the influences of the material properties of the wire electrode, such as surface tension and viscosity, on the droplet behavior in pulsed-MIG welding are also numerically investigated.

## 2 Simulation model

The model constructed in the present study includes the arc plasma, the metal transfer, and the weld pool. The simulation is carried out considering the interaction of these phenomena. Details of the simulation are available in a previous report [18]. A schematic diagram and the boundary conditions of the model used in the present paper are shown in Fig. 1. The model is a 2D axial-symmetric model, and the torch and the base metal are stationary. The arc current is provided from the top of the wire electrode, and the shielding gas flows into the calculation domain from the top boundary. The wire electrode is fed from the top boundary of the calculation domain, and its temperature at the top boundary is set to 300 K. The bottom

surface of the base metal is set to 300 K and grounded. The flow in both the arc plasma and the molten metal is treated as laminar flow. The governing equations used in this model are described as follows.

Under the local thermodynamic equilibrium (LTE) approximation, the arc plasma can be treated as an electromagnetic viscous fluid, and its behavior can be described by the following equations:

$$\nabla \cdot (\rho \vec{v}) = S \quad (1)$$

$$\frac{\partial (\rho \vec{v})}{\partial t} + \nabla \cdot (\rho \vec{v} \vec{v}) = -\nabla P + \nabla \cdot \tau + \rho \vec{g} + \vec{F}_{em} \quad (2)$$

$$\frac{\partial (\rho H)}{\partial t} + \nabla \cdot \rho \vec{v} H = -\nabla \cdot (-\kappa \nabla T) + W - Ra + S_E \quad (3)$$

where  $\vec{v}$  is the velocity [m/s],  $t$  is the time [s],  $\rho$  is the density [kg/m<sup>3</sup>],  $P$  is the pressure [Pa],  $\tau$  is the viscous stress tensor [Pa],  $\vec{g}$  is the gravitational acceleration [m/s<sup>2</sup>],  $H$  is the enthalpy [J/kg],  $\kappa$  is the thermal conductivity [W/m·K],  $T$  is the temperature [K],  $Ra$  is the radiative loss [W/m<sup>3</sup>],  $\vec{F}_{em}$  is the electromagnetic force [N/m<sup>3</sup>],  $W$  is the Joule heating [W/m<sup>3</sup>],  $S$  is the source term of mass by metal vapor [kg/m<sup>3</sup>s], and  $S_E$  is the source term of energy by metal vapor [W/m<sup>3</sup>].

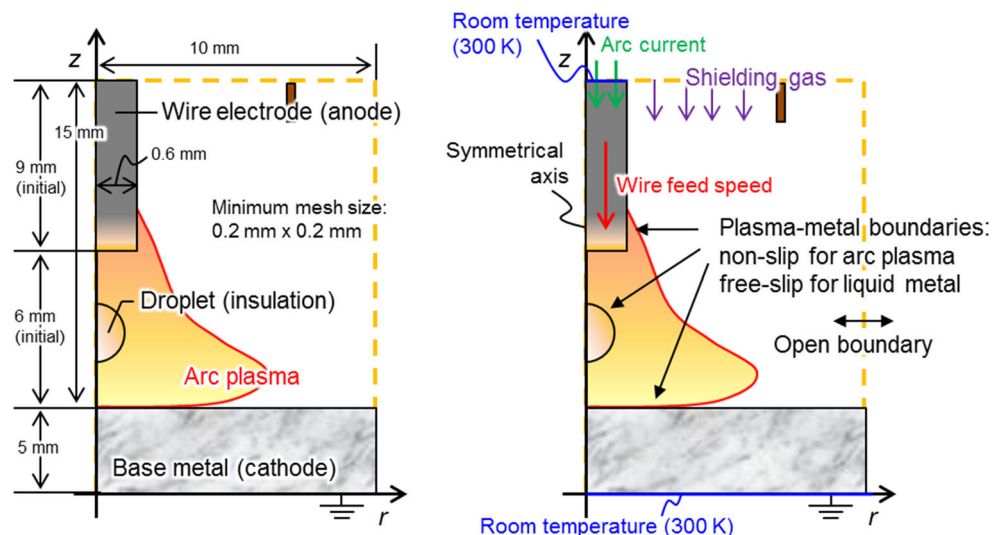
The electromagnetic force and the Joule heating can be calculated using the following equations:

$$\vec{F}_{em} = \vec{j} \times \vec{B} \quad (4)$$

$$W = \frac{|\vec{j}|^2}{\sigma} \quad (5)$$

where  $\vec{j}$  is the current density [A/m<sup>2</sup>],  $\vec{B}$  is the magnetic flux density [T], and  $\sigma$  is the electrical conductivity [S/m]. The

**Fig. 1** Schematic diagram and boundary conditions of the model used in the present study



current density and the magnetic flux density can be calculated using the following equations:

$$\nabla \cdot \vec{j} = 0 \tag{6}$$

$$\vec{j} = -\sigma \nabla V \tag{7}$$

$$\vec{B} = \nabla \times \vec{A} \tag{8}$$

$$\nabla^2 \vec{A} = -\mu_0 \vec{j} \tag{9}$$

where  $V$  is the electric potential [V],  $\vec{A}$  is the vector potential [N/A], and  $\mu_0$  is the permeability of free space [H/m].

In this model, the influence of iron vapor is taken into account. Iron vapor is only generated from the tip of the electrode and the droplet, and its distribution can be described using the following equation:

$$\frac{\partial(\rho C)}{\partial t} + \nabla \cdot (\rho \vec{v} C) = -\nabla \cdot (-\rho D \nabla C) + S \tag{10}$$

where  $C$  is the mass fraction of iron vapor and  $D$  is the diffusion coefficient [m<sup>2</sup>/s] [20]. The iron vapor is generated according to the Hertz-Knudsen-Langmuir equation [17, 21]:

$$J = \left( \frac{p_0}{\sqrt{T_{Metal}}} - \frac{p_{Fe,vap}}{\sqrt{T_{Gas}}} \right) \sqrt{\frac{M}{2\pi R}} \tag{11}$$

where  $J$  is the mass flux of iron vapor [kg/m<sup>2</sup>·s],  $p_0$  is the saturated vapor pressure of the iron vapor [Pa],  $p_{Fe,vap}$  is the partial pressure of iron vapor in the arc plasma [Pa],  $T_{Metal}$  is the temperature of the metal [K],  $T_{Gas}$  is the temperature of the arc plasma adjacent to the metal [K],  $M$  is the molecular weight of iron [kg/mol], and  $R$  is the gas constant [J/mol·K]. In Eqs. (1) and (3),  $S$  and  $S_E$ , respectively, were calculated using the following equations:

$$S = \nabla \cdot \vec{J} \tag{12}$$

$$S_E = H_{vap} \nabla \cdot \vec{J} \tag{13}$$

where  $H_{vap}$  is the vaporization heat of iron [J/kg],  $\vec{J} = -Jn$ , and  $n$  is the unit normal vector calculated from the shape of the metal. In this model, the shielding gas is argon, and the material properties of the plasma gas were taken from a paper by Murphy [21].

Next, the method for calculating droplet formation is explained. The governing equations of the metal region were as follows:

$$\nabla \cdot \vec{v} = -\frac{1}{\rho} S \tag{14}$$

$$\frac{\partial \vec{v}}{\partial t} + \nabla \cdot (\vec{v} \vec{v}) = -\frac{1}{\rho} \nabla P + \frac{1}{\rho} \nabla \cdot \boldsymbol{\tau} + \vec{g} + \vec{F}_{ex} \tag{15}$$

$$\frac{\partial H}{\partial t} + \nabla \cdot \vec{v} H = -\frac{1}{\rho} \nabla \cdot (-\kappa \nabla T) + \frac{1}{\rho} W - \frac{1}{\rho} S_E \tag{16}$$

where  $\vec{F}_{ex}$  is the external force vector [N/m<sup>3</sup>]. This is a summation of the electromagnetic force, the surface tension, the arc pressure, and the drag force by plasma stream.

Metal transfer and weld pool phenomena involve the deformation of a free surface, which was tracked in this model using the volume of fluid (VOF) method [22]. In the VOF method, the shape of a free surface is described by fluid occupancy using an  $F$  value for each calculation cell. According to the velocity field in the metal region, the free surface deformation is calculated using the following equation:

$$\frac{\partial F}{\partial t} + (\vec{v} \cdot \nabla) F = 0 \tag{17}$$

The surface tension force was calculated using the CSF model [23], in which the capillary pressure of surface tension acting on the liquid phase is expressed as a volume force in the surface region. This can be calculated as follows:

$$\vec{F}_{ST} = \gamma \kappa_{curv} \vec{n} \tag{18}$$

where  $\vec{F}_{ST}$  is the equivalent volume force vector of the capillary pressure of the surface tension [N/m<sup>3</sup>],  $\gamma$  is the surface tension [N/m],  $\kappa_{curv}$  is the curvature [1/m], and  $\vec{n}$  is the normal vector [1/m].

In this model, sheath regions formed near the wire electrode and the base metal are ignored. The wire electrode, which is an anode, and the base metal, which is a cathode, receive additional energy at their surface. These energy fluxes are given by following equations:

Wire electrode (anode):

$$\vec{q}_{Anode} = -\vec{j} \varphi_{Anode} - \varepsilon \alpha T_{Metal}^4 \vec{n} \tag{19}$$

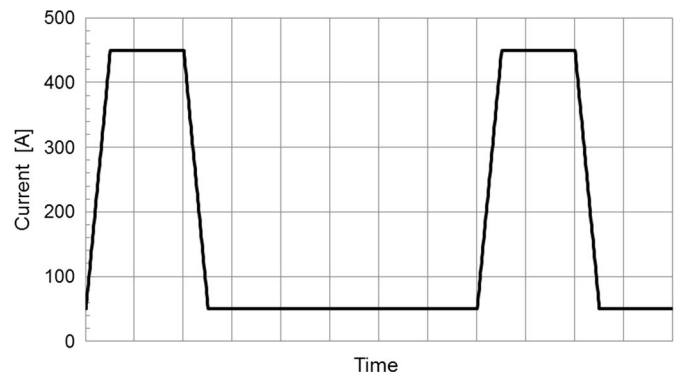
Base metal (cathode):

$$\vec{q}_{Cathode} = -\vec{j}_e \varphi_{Cathode} + \vec{j}_i V_i - \varepsilon \alpha T_{Metal}^4 \vec{n} \tag{20}$$

where  $\vec{q}_{Anode}$  and  $\vec{q}_{Cathode}$  are the energy fluxes at the anode and cathode surfaces [W/m<sup>2</sup>], respectively,  $\varphi_{Anode}$  and  $\varphi_{Cathode}$  are the work functions of an anode and cathode [V], respectively,  $\vec{j}_i$  and  $\vec{j}_e$  are the ion and electron current

**Fig. 2** Waveform of pulse current used in simulation

Pulse parameters	
Peak current:	450 A
Base current:	50 A
Average current:	150 A
Peak time:	0.5~4.0 ms
Rise time:	0.5 ms
Fall time:	0.5 ms



densities [ $A/m^2$ ], respectively,  $\varepsilon$  is the radiative emissivity, and  $\alpha$  is the Stefan-Boltzmann coefficient [ $W/m^2 \cdot K^4$ ]. The electron current density is calculated using the Richardson-Dushman equation and the ion current density is determined by subtracting the electron current density from the total current density.

### 3 Simulation conditions

Figure 2 shows the pulse waveform used in the simulation. A trapezoidal pulsed current is used in this simulation. In the present study, the base and peak currents are set to 50 and 450 A, respectively. The influence of the peak time on the metal transfer phenomena is numerically investigated. The base time (time between pulses) is adjusted so that the average current is 150 A. The wire diameter is 1.2 mm, and the distance between the contact tip and the base metal is set to 15 mm. The wire feed rate is set to 360 cm/min. The wire feed rate is adjusted to maintain the initial arc length in this model, and this value is used in all calculations in this paper. The wire electrode and the base metal are mild steel, and the material

properties used in this model are listed in Table 1 [24, 25]. In order to simplify the phenomena, only the thermal conductivity and the specific heat of the metal depend on the temperature, and temperature dependence of other properties is ignored. In addition, in the present study, in order to investigate the influence of the material properties of the wire electrode, we also perform the calculation using various values of surface tension and viscosity.

### 4 Simulation results

#### 4.1 Initial conditions

First, the initial conditions of the calculation in the present study are explained. The initial conditions of the metal region are fixed, as shown in Fig. 3a. The temperature of the base metal is set to room temperature (300 K). The initial

**Table 1** Physical properties of mild steel

Density ( $kg/m^3$ )	7200
Viscosity (Pas)	$6 \times 10^{-3}$ (standard), $3 \times 10^{-3}$ , $9 \times 10^{-3}$
Thermal conductivity (W/mK)	26 to 52
Specific heat (j/kgK)	695 to 800
Electric conductivity (S/m)	$7.7 \times 10^5$
Surface tension (N/m)	1.2 (standard), 0.6, 1.8
Work function (V)	4.3
Melting temperature (K)	1750
Latent heat of fusion (J/kg)	$2.47 \times 10^5$
Boiling temperature (K)	3080
Latent heat of vaporization (J/kg)	$7.34 \times 10^6$
Radiation emissivity	0.4

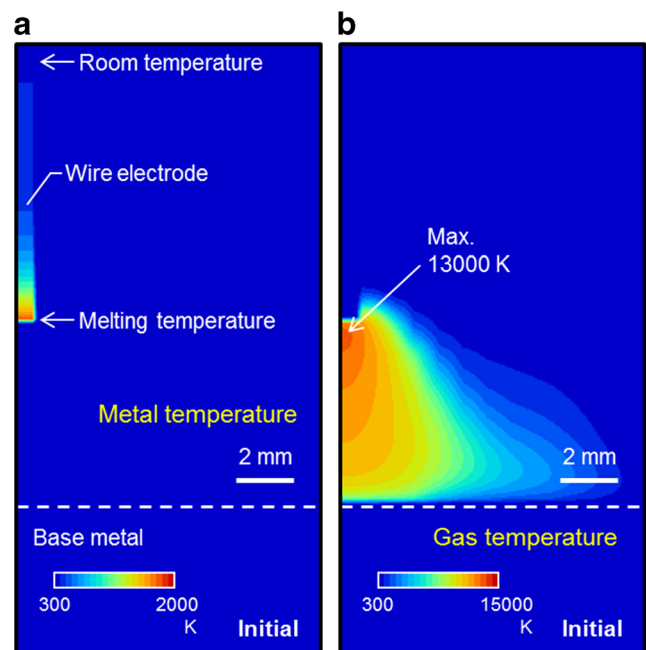


**Fig. 3** Initial conditions of calculation. **a** Metal temperature. **b** Gas temperature

temperature of the wire electrode is room temperature at the contact tip and melting temperature at the bottom tip. The initial conditions of the arc plasma are calculated until a steady state is reached using the initial conditions of the metal region using a base current of 50 A. Figure 3b shows the initial conditions of the gas region. For such initial conditions, the metal temperature is low, so metal vapor is hardly generated.

### 4.2 Influence of the peak time on metal transfer

Figure 4 shows the calculation results when the peak time is set to 1.5 ms. In this calculation, the surface tension is 1.2 N/m, and the viscosity is  $6 \times 10^{-3}$  Pa·s. The results reveal the temperature fields of the arc plasma and the metal region, as well as the iron vapor concentration distribution,

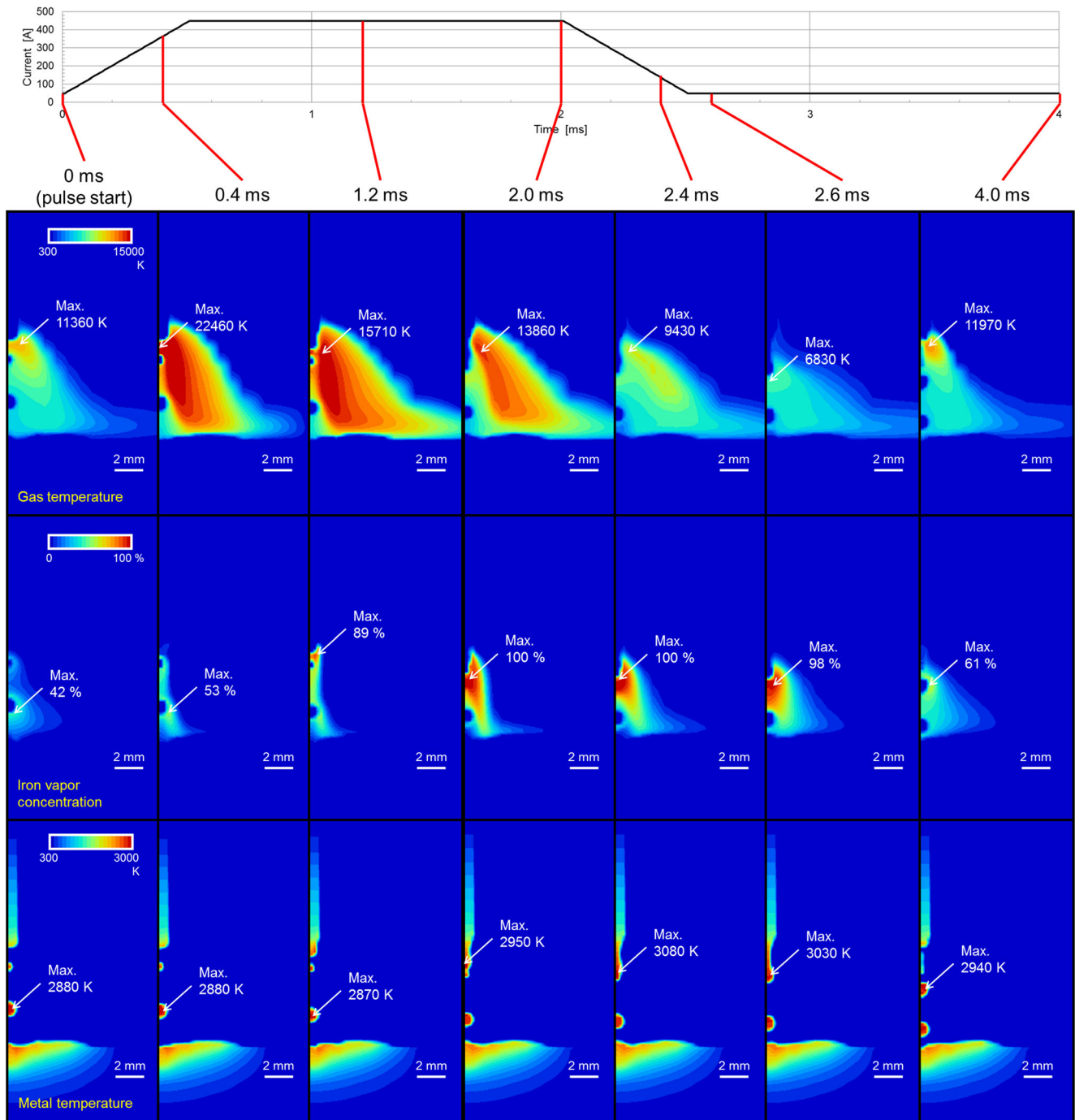


**Fig. 4** Time evolution of the temperature field of the arc plasma and iron vapor concentration distributions and of the temperature field of the metal region (peak time 1.5 ms)



approximately 400 ms after the initial conditions. In this case, periodic behavior is observed in the calculation. In the figure, the start of the rising edge of the pulse is set as 0 ms. Moreover, just after the pulse reaches its peak amplitude, the temperature of the arc plasma and the tip of the wire electrode rapidly increases, and the droplet begins to grow. In the latter half of the peak duration, the temperature of the droplet at the wire tip becomes high, and a large amount of metal vapor is generated and flows into the center of the arc plasma. Consequently, the temperature at the center of the arc plasma becomes low because the radiation loss of the iron vapor is very strong [26]. After the end of the peak duration, the arc plasma temperature becomes low, and the droplet detaches from the wire tip. The concentration of the metal vapor also decreases. Under these conditions, only one droplet is transferred per pulse, i.e., one-pulse, one-droplet transfer is obtained. Here, one-pulse, one-droplet transfer is also obtained in the experiment using the same pulse current. It is difficult to compare the values of the temperature and the iron vapor concentration, but these distributions of the numerical results are similar to those of the experimental results [27].

The relationship between the current and the behavior of the arc plasma and the droplet is summarized in Figs. 5 and 6. As shown in Fig. 5a, when the pulse reaches its peak amplitude, the maximum temperature of the arc plasma increases rapidly, but then decreases rapidly. After the middle of the

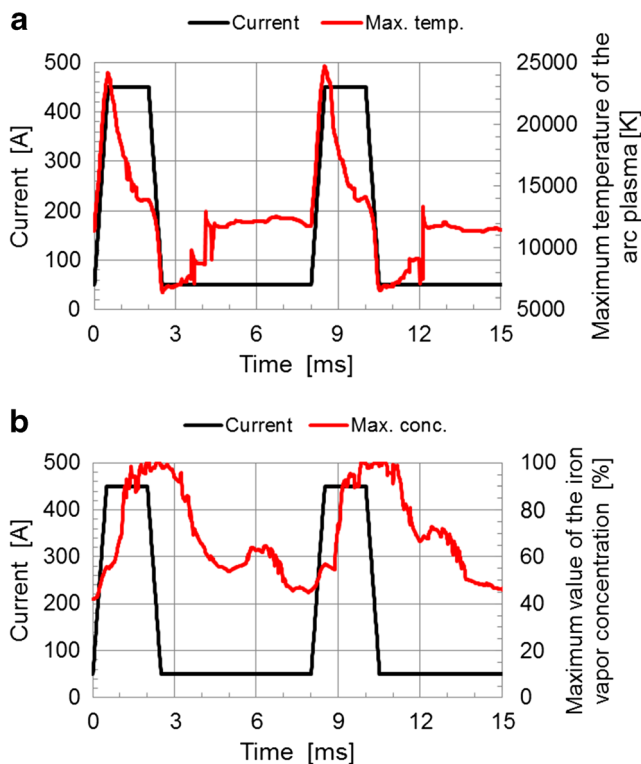


**Fig. 5** Time evolution of the maximum temperature and iron vapor concentration in the arc plasma. **a** The maximum temperature of the arc plasma. **b** The maximum value of the iron vapor concentration

peak duration, the peak temperature of the arc plasma is relatively low. This behavior is closely related to the iron vapor. The maximum value of the iron vapor concentration rapidly increases at the middle stage of the peak shown in Fig. 5b. When the concentration of the iron vapor becomes higher, the radiation loss from the arc plasma becomes larger and the temperature decreases. On the other hand, considering the behavior of the droplet, the surface temperature increases gradually while the pulse is at its peak amplitude, as shown in Fig. 6a, and the evaporation rate of the iron vapor increases rapidly at the middle of the peak, as shown in Fig. 6b. Based on these results, the behavior can be summarized as follows. When the peak duration is started, the temperature of the arc plasma increases rapidly at first. Then, the heat input into the wire tip becomes large, and the temperature of the droplet and the evaporation rate of the iron vapor increase. The concentration of the iron vapor then becomes higher, and the temperature of the arc plasma decreases. This behavior is synchronized with the current, as shown in the figures. Therefore, under the one-pulse, one-droplet transfer condition, not only the droplet but also the arc plasma and the metal vapor exhibit periodic behavior.

Figure 7 shows the relationship between the peak time and the number of the droplets transferred in one pulse. Here, very small droplet whose size is smaller than the mesh size is ignored in counting the number of droplets. As shown in this figure, when the peak time is 1.5–3.0 ms, the one-pulse, one-droplet transfer is obtained.

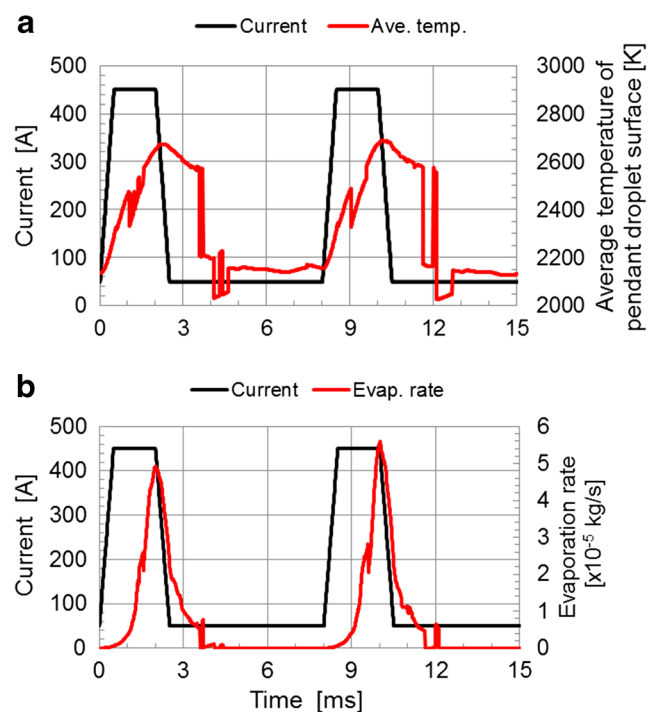


**Fig. 6** Time evolution of the evaporation rate and surface temperature of the droplet. **a** The surface temperature of the pendant droplet. **b** The evaporation rate of iron vapor

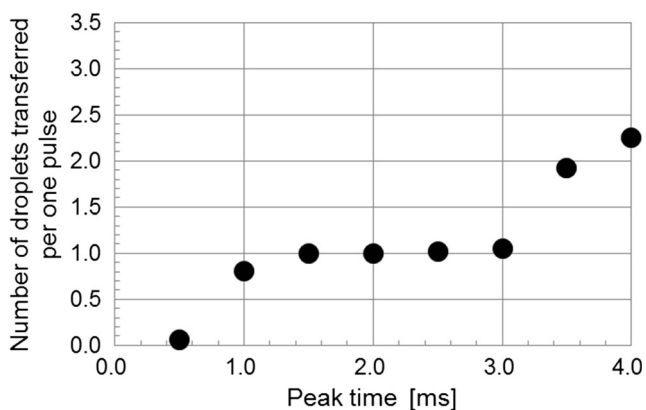


**Fig. 7** Influence of peak time on the number of droplets transferred per pulse

Thus, the peak time for one-pulse, one-droplet transfer condition has a certain range. When the peak time becomes shorter, more than one pulse is required to transfer one droplet (“n-pulse, one-droplet” transfer condition). On the other hand, when the peak time becomes longer, more than one droplet is transferred in one pulse (“one-pulse, n-droplet” transfer).

#### 4.3 Influence of the material properties of wire on metal transfer

The influences of the surface tension and viscosity of the wire electrode on the metal transfer are shown. Figure 8a shows the relationship between the peak time and the number of droplets transferred during one pulse for various surface tensions. The influence of the viscosity is shown in Fig. 8b. The simulation results change only slightly with the viscosity, so the influence of the viscosity is weak. In contrast, the number of droplets transferred per pulse changes significantly with the surface tension. When the surface tension decreases, the range of the peak time for obtaining one-pulse, one-droplet transfer is reduced. The surface tension of the wire electrode strongly depends on its composition and temperature. The value of the surface tension of the pure iron at the melting point is around 1.9 N/m, and it decreases when the temperature becomes higher. In addition, when the surface-active element such as oxygen or sulfur exists, the value of the surface tension significantly decreases [28]. The balance between the surface tension and the electromagnetic force is very important to determine the droplet behavior in pulsed-MIG welding. In the case of lower surface tension, the force holding up the droplet becomes weaker. Consequently, the electromagnetic force acting to detach the droplet becomes stronger relatively. Therefore, the simulation results revealed that the material properties of the electrode wire strongly affect the properties of the metal transfer. It is very important to consider both the

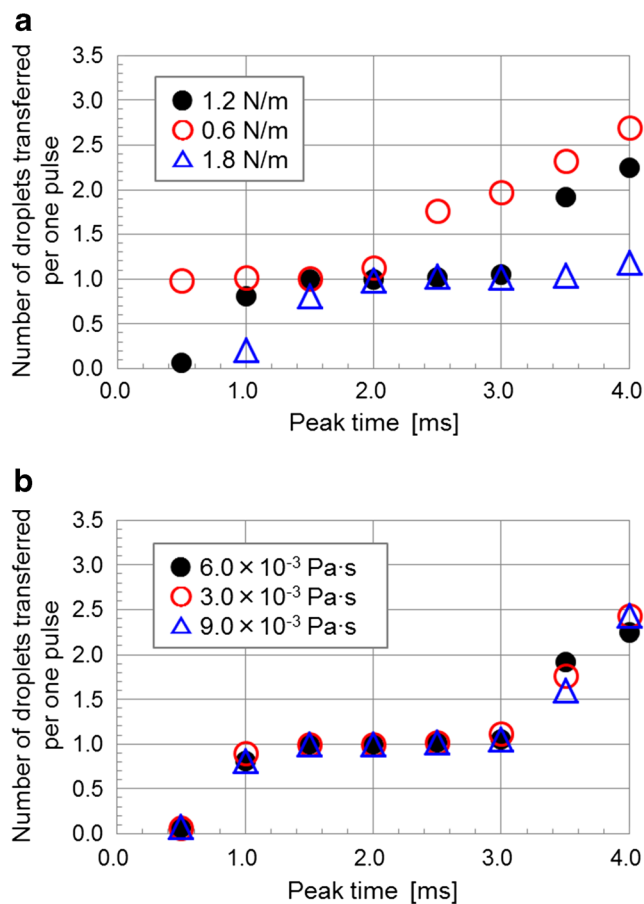


**Fig. 8** Influence of material properties on the number of droplets transferred per pulse. **a** Surface tension. **b** Viscosity

properties of the power source and the weld material in order to control the overall welding process.

## 5 Conclusion

In the present study, the metal transfer phenomena in pulsed-MIG welding were visualized and discussed based on numerical simulation results. The results obtained in the present study are as follows:

1. When using a trapezoidal pulse current with base and peak currents of 50 and 450 A, respectively, one-pulse, one-droplet transfer is achieved when the peak time is set between 1.5 and 3.0 ms.
2. Under the one-pulse, one-droplet transfer condition, not only the droplet but also the arc plasma and the metal vapor exhibit periodic behavior.
3. The viscosity of the electrode wire has almost no influence on the metal transfer, but the surface tension strongly affects the metal transfer. The balance between the surface tension and the electromagnetic force is very important to determine the droplet behavior in pulsed-MIG welding. In

controlling the overall welding process, it is very important to consider both the properties of the power source and the weld material.

**Acknowledgments** This research was supported by the Structural Materials for Innovation of the Cross-ministerial Strategic Innovation Promotion Program (SIP) of Japan Science and Technology (JST), and JSPS KAKENHI Grant Number JP16H06937.

## References

- Kim Y-S, Eagar TW (1993) Metal transfer in pulsed current gas metal arc welding. *Weld J* 72:279s–287s
- Hirata Y (2003) Pulsed arc welding. *Weld Int* 17(2):98–115
- Ueyama T, Ohnawa T, Tanaka M, Nakata K (2007) Occurrence of arc interaction in tandem pulsed gas metal arc welding. *Sci Technol Weld Join* 12(6):523–529
- Greene WJ (1960) An analysis of transfer in gas-shielded welding arc. *Trans AIEE Part 2* 7:194–203
- Amson JC (1965) Lorentz force in the molten tip of an arc electrode. *Br J Appl Phys* 16:1169–1179
- Waszink JH, Graat LHM (1983) Experimental investigation of forces acting on a drop of weld metal. *Weld J* 62:108s–116s
- Allum CJ (1985) Metal transfer in arc welding as a varicose instability: I. Varicose instabilities in a current-carrying liquid cylinder with surface tension. *J Phys D Appl Phys* 18:1431–1446
- Allum CJ (1985) Metal transfer in arc welding as a varicose instability: I. Development of model for arc welding. *J Phys D Appl Phys* 18:1447–1468
- Simpson SW, Zhu P (1995) Formation of molten droplet at a consumable anode in an electric welding arc. *J Phys D Appl Phys* 28:1594–1600
- Choi SK, Yoo CD, Kim Y-S (1998) Dynamic simulation of metal transfer in GMAW, part 1: globular and spray transfer modes. *Weld J* 77:38s–44s
- Choi SK, Yoo CD, Kim Y-S (1998) The dynamic analysis of metal transfer in pulsed current gas metal arc welding. *J Phys D Appl Phys* 31:207–215
- Wang G, Huang PG, Zhang YM (2003) Numerical analysis of metal transfer in gas metal arc welding. *Metall Mater Trans B* 34B:345–353
- Kadota K, Hirata Y (2011) Numerical model of metal transfer using an electrically conductive liquid. *Weld World* 55(09/10):50–55
- Haidar J, Lowke JJ (1996) Predictions of metal droplet formation in arc welding. *J Phys D Appl Phys* 29:2951–2960
- Hu J, Tsai HL (2007) Heat and mass transfer in gas metal arc welding. Part II: the metal. *Int J Heat Mass Transf* 50:808–820
- Xu G, Hu J, Tsai HL (2009) Three-dimensional modeling of arc plasma and metal transfer in gas metal arc welding. *Int J Heat Mass Transf* 52:1709–1724
- Hertel M, Spille-Kohoff A, Fuessel U, Schnick M (2013) Numerical simulation of droplet detachment in pulsed gas-metal arc welding including the influence of metal vapour. *J Phys D Appl Phys* 46:224003
- Ogino Y, Hirata Y, Murphy AB (2016) Numerical simulation of GMAW process using Ar and an Ar-CO<sub>2</sub> gas mixture. *Weld World* 60:345–353
- Ogino Y, Hirata Y (2015) Numerical simulation of metal transfer in argon gas-shielded GMAW. *Welding in the World* 59:465–473
- Wilke CR (1950) A viscosity equation for gas mixtures. *J Chem Phys* 18(4):517–519
- Murphy AB (2010) The effect of metal vapour in arc welding. *J Phys D Appl Phys* 43:434001
- Hirt CW, Nichols BD (1981) Volume of fluid (VOF) method for the dynamics of free boundaries. *J Comput Phys* 39:201–225
- Brackbill JU, Kothe DB, Zang CA (1992) A continuum method for modeling surface tension. *J Comput Phys* 100:335–354
- Rao ZH, Hu J, Liao SM, Tsai HL (2010) Modeling of the transport phenomena in GMAW using argon–helium mixtures. Part I—the arc. *Int J Heat Mass Transf* 53:5707–5721
- Ushio M, Wu CS (1997) Mathematical modeling of three-dimensional heat and fluid flow in a moving gas metal arc weld pool. *Metall Mater Trans B* 28B:509–516
- Schnick M, Fuessel U, Hertel M, Haessler M, Spille-Kohoff A, Murphy AB (2010) Modelling of gas-metal arc welding taking into account metal vapour. *J Phys D Appl Phys* 43:434008
- Shigeta M, Nakanishi S, Tanaka M, Murphy AB (2017) Analysis of dynamic plasma behaviours in gas metal arc welding by imaging spectroscopy. *Weld Int*. doi:10.1080/09507116.2016.1223220
- Keene BJ (1993) Review of data for the surface tension of pure metals. *Int Mater Rev* 38(4):157–192